Polymer 54 (2013) 5310–5320

Contents lists available at ScienceDirect

Polymer

journal homepage: www.elsevier.com/locate/polymer

Polyurethaneurea–silica nanocomposites: Preparation and investigation of the structure–property behavior

Ozge Malay [a], Oguzhan Oguz [a], Cagla Kosak [b], Emel Yilgor [b], Iskender Yilgor [b,**], Yusuf Z. Menceloglu [a,*]

[a] Advanced Composites and Polymer Processing Laboratory, Faculty of Engineering and Natural Sciences, Sabancı University, Tuzla 34956, Istanbul, Turkey
[b] Surface Science and Technology Center, KUYTAM, Chemistry Department, Koc University, 34450 Sariyer, Istanbul, Turkey

ARTICLE INFO

Article history:
Received 6 April 2013
Received in revised form
3 July 2013
Accepted 19 July 2013
Available online 26 July 2013

Keywords:
Nanocomposite
Thermoplastic polyurethane–urea
Silica nanoparticles

ABSTRACT

Nanocomposites consisting of thermoplastic polyurethane–urea (TPU) and silica nanoparticles of various size and filler loadings were prepared by solution blending and extensively characterized by Fourier transform infrared (FTIR) spectroscopy, scanning electron microscopy (SEM), thermal analysis, tensile tests, and nanoindentation. TPU copolymer was based on a cycloaliphatic diisocyanate and poly(tetramethylene oxide) (PTMO-2000) soft segments and had urea hard segment content of 20% by weight. TPU/silica nanocomposites using silica particles of different size (29, 74 and 215 nm) and at different loadings (1, 5, 10, 20 and 40 wt. %) were prepared and characterized. Solution blending using isopropyl alcohol resulted in even distribution of silica nanoparticles in the polyurethane–urea matrix. FTIR spectroscopy indicated strong interactions between silica particles and polyether segments. Incorporation of silica nanoparticles of smaller size led to higher modulus and tensile strength of the nanocomposites, and elastomeric properties were retained. Increased filler content of up to about 20 wt. % resulted in materials with higher elastic moduli and tensile strength while the glass transition temperature remained the same. The fracture toughness increased relative to neat TPU regardless of the silica particle size. Improvements in tensile properties of the nanocomposites, particularly at intermediate silica loading levels and smaller particle size, are attributed to the interactions between the surface of silica nanoparticles and ether linkages of the polyether segments of the copolymers.

1. Introduction

Polymeric nanocomposites have received widespread attention due to their enhanced physical, chemical and engineering properties and potential use in diverse fields of applications. Polymeric nanocomposites are mostly prepared by homogeneous dispersion of nanosized inorganic fillers within an organic polymeric matrix [1]. A wide range of polymeric nanocomposites has been prepared by using different polymer matrices (thermoplastic or thermoset) and inorganic fillers (organoclays, fumed silica, carbon nanofibers or nanotubes, graphene) [2–7]. The reinforcing effect of different classes of fillers depends mainly on; (i) particle structure, size and shape, (ii) loading concentration, (iii) strength of the matrix–filler interaction and (iv) distribution of the particles within the matrix. An important factor that influences the distribution of the fillers within the matrix is the preparation method of the nanocomposites, which could be melt-processing [8], solution blending [9] or in-situ polymerization [10].

Segmented thermoplastic polyurethanes, polyureas and poly(urethane–urea)s (TPU) constitute an important class of linear-segmented block copolymers with alternating hard and soft segments. In TPUs soft segments are usually medium to high molecular weight (M_n ~ 1000–3000 g/mol) α,ω-dihydroxy or α,ω-diamine terminated oligomers with glass transition (T_g) or softening temperatures well below room temperature (such as aliphatic polyethers and polyesters, polyisobutylene, polydimethylsiloxane). Hard segments are generally formed by the reaction of the diisocyanate with a low molecular weight diol (urethane) or diamine (urea), through the so-called chain extension reactions [11,12]. Due to the thermodynamic incompatibility between the soft and the hard segments TPUs display phase separated morphologies or nanostructures [11,13,14]. Strong hydrogen bonding between the urethane or urea type hard segments leads to the formation of a physically crosslinked network, which strongly contributes to the interesting combination of properties of TPUs. Due to strong

* Corresponding author. Tel.: +90 216 483 9501; fax: +90 216 483 9550.
** Corresponding author. Tel.: +90 212 338 1418; fax: +90 212 233 81559.
E-mail addresses: iyilgor@ku.edu.tr (I. Yilgor), yusufm@sabanciuniv.edu (Y.Z. Menceloglu).

0032-3861/$ – see front matter © 2013 Elsevier Ltd. All rights reserved.
http://dx.doi.org/10.1016/j.polymer.2013.07.043

hydrogen bonded hard segments dispersed in a continuous soft matrix, TPUs are regarded as 'self-reinforcing' materials.

Polyester soft segment based TPUs find applications in wire insulation, automobile fascia, footwear (lifts, ski boots, football cleats), wheels (industrial, skateboard), and adhesives [12]. In general, polyesters produce much tougher TPUs with a better range of physical properties when compared with their polyether based homologs. Major advantages offered by polyether based TPUs are superior low temperature flexibility and improved hydrolytic stability [14,15]. Lately, there is a growing interest to broaden the range of applications for polyether based TPUs beyond the current limits by the addition of nanosized fillers. Recently, several studies have shown that mechanical and thermal properties of TPUs can be improved through the preparation of nanocomposites. However, most of these studies are conducted on polyester based TPUs, where organo-modified silicates [8,16,17], carbon nanotubes [18–20], carbon nanofibers [21,22] and fumed silica nanoparticles [23–26] were used as fillers.

In TPU based nanocomposites there is only a limited number of studies that address the use of colloidal silica especially for the polyether-based materials. In these studies, silica sol was either blended with polyol (prior to the reaction with diisocyanate) [27–30] or added to monomers at the stage of polyester preparation by polycondensation [31] to avoid agglomeration of the particles. Recently, polyether based polyurethane/silica nanocomposites were prepared by using sol–gel process. These crosslinked hybrid nanocomposites were obtained by adding fumed silica directly [32] or dispersed in a solvent [33] into organoalkoxysilane end-capped prepolymer solutions. On the other hand, there is no report in the literature dealing with the use of silica sol "as synthesized and aged" in basic media for the preparation of polyether-based TPU/silica nanocomposites, specifically through solution blending of the copolymer and the silica sol.

The central theme of this study is to systematically investigate the reinforcing effect of silica nanoparticles in well-defined polyether-based TPU/silica nanocomposites. For this purpose, a bottom-up approach was applied. Silica sols containing average particle size in 29–215 nm range were prepared by Stöber method [34]. Poly(-tetramethylene oxide) based segmented urethaneurea copolymer with a hard segment content of 20% by weight was synthesized in our laboratories. Nanocomposites with silica loadings of 1–40% by weight and with silica sizes from 29 to 214 nm were prepared by mixing the copolymer solution and the colloidal silica, prepared in a common organic solvent. The effects of silica concentration and particle size on physical, thermal and mechanical properties of the resultant polyurethane–urea nanocomposites were investigated.

2. Experimental

2.1. Materials

Poly(tetramethylene oxide)glycol (PTMO-2K) with $<M_n>$ = 2040 g/mol and diamine chain extender 2-methyl-1,5-diamino pentane (MDAP) were kindly provided by DuPont. The diisocyanate, bis(4-isocyanatocyclohexyl)methane (HMDI) was kindly supplied by Bayer and had a purity better than 99.5%. Dibutyltin dilaurate (DBTDL) was obtained from Witco and is used as a catalyst by diluting to 1 wt. % in tetrahydrofuran. Reagent grade 2-propanol (IPA) and tetrahydrofuran (THF), aqueous ammonia solution (NH_4OH, 25%) and tetraethylortosilicate (TEOS, >99%) were obtained from Merck. All chemicals were used as received.

2.2. Synthesis and characterization of PTMO based polyurethaneurea copolymer

Polyurethaneurea segmented copolymers with 20% by weight hard segment content were synthesized by using the two-step polymerization procedure, called the "prepolymer method". All reactions were carried out in three-neck, round bottom, Pyrex reaction flasks equipped with a mechanical overhead stirrer, a thermometer and an addition funnel. Temperature control was provided by a heating mantle. For the preparation of isocyanate terminated prepolymer, calculated amounts of PTMO-2K and HMDI were introduced into the reaction flask, heated to 80 °C and stirred in bulk. 150 ppm of DBTDL (1 weight% solution in THF) was used as a catalyst. Prepolymer formation reaction was monitored by Fourier transform infrared spectroscopy (FTIR). Prepolymer reactions were completed in about 1 h. The heat was then turned off and the prepolymer was dissolved in THF to make a solution with a solids content of about 80% by weight. The solution was then cooled down to room temperature and further diluted with IPA to make a 60% solution. Chain extension reaction was performed at room temperature by the dropwise addition of MDAP solution in IPA (20% solids) onto the prepolymer solution. As the polymer molecular weight and the viscosity of the solution increased, the system was diluted with THF/IPA mixture (7/3 by volume) to a final solids content of about 20% by weight. Completion of the reaction was determined by FTIR spectroscopy by monitoring the disappearance of the strong isocyanate peak at 2260 cm^{-1}. The polyurethaneurea solution obtained was cast in a Teflon mold. The mold was kept at room temperature for 24 h and then placed in a vacuum oven at 60 °C for 24 h for complete evaporation of the solvent.

Gel permeation chromatography (GPC) measurements were performed on a Viscotek VE 2001 series instrument equipped with four columns (2×T3000, T2000 and TGuard) and Viscotek VE 3580 refractive index detector. DMF was used as the mobile phase at 50 °C with a flow rate of 1 mL/min. Polymer samples were prepared at a concentration of 1–2 mg/mL in DMF. Molecular weights were determined from calibration curves plotted from narrow molecular weight polystyrene standards.

2.3. Preparation and characterization of silica sol

Silica sols were prepared in basic medium by using sol–gel method [34]. In conventional basic sol–gel systems, ethanol is used as the parent alcohol when TEOS is employed as the precursor. However, in this study, we used isopropanol (IPA) as the solvent to enhance the compatibility and mixing conditions of the silica sol and the polyurethaneurea copolymer, which is soluble in a THF/IPA solvent mixture.

Sol–gel reactions were carried out in 100 mL glass reactors with low to moderate mixing speeds at room temperature (25 ± 2 °C). Initially, IPA and aqueous ammonia were mixed and ultrasonicated for 20 min, and then TEOS was quickly poured into the reactor to initiate the reaction. Silica sols of various particle size were prepared at molar ratios of $[TEOS]/[NH_3]_{aq}$ = 0.8, 1.7 and 2.8 and denoted as S1, S2 and S3, respectively.

Hydrodynamic diameter and size distribution of silica nanoparticles in 2-propanol and zeta potential of silica sols were analyzed with Dynamic Light Scattering (DLS) Zetasizer Nano (Malvern, UK). Transmission electron microscopy (TEM) analysis was performed using a Philips-FEI Tecnai G2 F20 S-Twin at 200 kV accelerating voltage in order to investigate the distribution of silica nanoparticles in copolymer. A drop of silica sol was deposited on carbon coated Lacey formvar films supported in 300 mesh copper grids (Ted Pella). The grid then was allowed to air-dry for 5 min and oven-dry at 50 °C for 15 min.

2.4. Preparation of nanocomposites

Silica/TPU nanocomposites were prepared by dissolving PTMO-based TPU in THF/IPA (10% solids by weight) and then adding the

silica sols. The mixture was stirred on a magnetic stirrer until a homogeneous distribution is ensured. To obtain thin films (0.3–0.5 mm) the solutions were cast into Teflon molds and the solvent was evaporated first at room temperature and then in a vacuum oven at 50 °C until complete drying.

2.5. Characterization of nanocomposites

IR spectra. FTIR spectra were recorded on a Thermo Scientific Nicolet Impact 400D Spectrometer. Solutions were cast on KBr discs and films were obtained after evaporating the solvent with an air gun. 32 scans were taken for each spectrum with a resolution of 2 cm^{-1}. Omnic 6.0 Software is used to monitor/analyze the spectra. ATR-IR spectra were recorded on a thermo scientific Smart iTR Instrument with Diamond ATR crystal and with an incident angle of 42° Omnic Software is used to monitor the spectra. 16 scans were taken for each spectrum with a resolution of 4 cm^{-1}.

Imaging. Field-emission Scanning Electron Microscopy (FE-SEM) (SUPRA 35VP, LEO, Germany) was used to investigate the morphology of the composite films. The films were fractured in liquid nitrogen and the fracture surfaces (cross-section) were coated with a thin layer of carbon prior to SEM examinations. TPU/silica blend deposited and dried on carbon coated Lacey formvar films was also imaged by TEM.

Thermal characterization. Thermal behavior of nanocomposites was analyzed by DSC 204 Phoenix Differential Scanning Calorimetry (Netzsch, Germany) between −160 and 80 °C, under N_2 atmosphere and at a heating and cooling rate of 10 °C/min. Thermogravimetric analyses were carried out using STA 449C simultaneous thermal analyzer (Netzsch, Germany) under nitrogen atmosphere with a heating rate of 10 °C/min, from ambient temperature to 900 °C.

Mechanical tests. Stress–strain tests were performed on an Instron model 4411 tester. Dog-bone specimens (ASTM D 1708) were punched out of the films. Tensile tests were performed with a crosshead speed of 25.0 mm/min (L_o = 24.0 mm). Tests were conducted at room temperature and for each polymer at least three specimens were tested. Hysitron TI 950 TriboIndenter nanomechanical test instrument was used to perform quasi-static indents on the samples. Displacement-controlled quasi-static tests were performed on the samples using a diamond Berkovich probe.

3. Results and discussion

Segmented TPUs are complex multi-phase materials due to their intrinsic structural heterogeneity arising from the differences in the solubility parameters of the hard (HS) and the soft (SS) segments and nature and strength of the inter and intramolecular interactions between HS and SS. In general the morphology of TPUs containing 20–25% by weight HS consists of spherical HS domains distributed in the elastomeric SS matrix. The aim of this study is the preparation and characterization of silica nanoparticle filled polyurethane–urea copolymers. To achieve this, silica nanoparticles with average particle sizes in 29–215 nm range were synthesized and utilized. PTMO based polyurethane–urea copolymer with an HS content of 20% by weight was prepared by using a cycloaliphatic diisocyanate (HMDI) and a short diamine (2-methyl-1,5-diaminopentane) chain extender and a two-step polymerization reaction called the prepolymer method. PTMO with an average molecular weight $<M_n>$ = 2040 g/mol was used as the soft segment. GPC analyses showed that the resultant polymer had number and weight average molecular weights of $<M_n>$ = 65,000 g/mol and $<M_w>$ = 116,000 g/mol with a PDI of 1.78. Primary focus of this study was to investigate the nature and extent of interactions between silica nanoparticles employed as fillers with the soft and/or hard segments of the polyether based thermoplastic polyurethane–urea copolymer. In addition, the effect of the size and the amount of the silica incorporation on thermal, mechanical and morphological properties of TPU/silica nanocomposites were also investigated.

3.1. Preparation and properties of the colloidal silica

Colloidal silica with three different particle sizes were prepared by the reaction of TEOS and dilute aqueous ammonium hydroxide in isopropanol at 25 °C, using Stöber method [34]. Table 1 shows the reaction stoichiometry employed and the size and size distribution of silica sols obtained with their stability provided by zeta potential measurements. DLS was used to determine the average size and the size distribution of silica particles. Average hydrodynamic diameters of three sets of silica particles were 29, 74 and 215 nm with respect to variations in the aqueous ammonia concentration. Particle size distribution in silica sols decreased with particle size and exhibited an almost monodisperse distribution for S2 and S3. Zeta potential values of silica sols were lower than critical stability limit of −30 mV with larger particles showing greater zeta potential values than smaller particles.

TEM images of the silica nanoparticles are provided in Fig. 1. The average particle diameter of silica nanoparticles determined by TEM was 18, 50 and 175 nm. Significantly smaller particle size determined by TEM pointed out profound particle shrinking due to dehydration under high vacuum condition.

Fig. 2 provides the FTIR spectra of the silica powders, which were dried after aging the silica sols for 4 days. The IR spectra of synthesized silica nanoparticles respectively show asymmetric stretching bands of Si–O–Si and Si–OH groups at 1040 and 960 cm^{-1} respectively. Furthermore, broad stretching bands in 3300–3500 cm^{-1} range are due to the surface hydroxyl (O–H) groups hydrogen bonded with water molecules on the silica surface. Asymmetric stretching bands of $-CH_3$ and $-CH_2$ at 2976 and 2930 cm^{-1}, respectively, indicate the presence of unhydrolyzed ethoxy groups ($-OCH_2CH_3$) on the silica surface. Apparently, ethoxy replacement by hydroxyl groups is more complete under higher ammonia concentration, which leads to greater extent in silanol condensation and bigger particles. These observations have vital effects on the mechanical properties of silica nanoparticles. Smaller silica particles, which are more ethoxylated, are less densely cross-linked and could be plasticized by the swelling solvents [35]. This is more noticeable when they are incompletely dried.

3.2. Composition and the morphology of the nanocomposites

Table 2 gives the compositions of the TPU/silica nanocomposites prepared in this study. In the coding TPU-20 indicates a polyurethaneurea with a hard segment content of 20% by weight,

Table 1
Properties of the colloidal silica (and sols) incorporated in TPU/silica nanocomposites.

Sample	$[TEOS]/[NH_3]_{aq}$	D_{DLS}[a] (nm)	D_{TEM}[b] (nm)	PdI_{DLS}[c]	ζ_{DLS}[d] (mV)
S1	2.8	29 ± 0.7	18 ± 3.0	0.3 ± 0.02	−67 ± 8.8
S2	1.7	74 ± 0.2	50 ± 7.2	0.1 ± 0.03	−74 ± 7.1
S3	0.8	215 ± 3.3	175 ± 25	0.04 ± 0.03	−87 ± 2.3

[a] Hydrodynamic radius measured by dynamic light scattering (DLS).
[b] Average particle diameter detected by transmission electron microscopy (TEM).
[c] Polydispersity index calculated from a cumulants analysis of the DLS measured intensity autocorrelation function. PdI is an indication of variance in the sample and given in the range [0,1].
[d] Zeta potential of colloidal sol measured by DLS Zetasizer Nano.

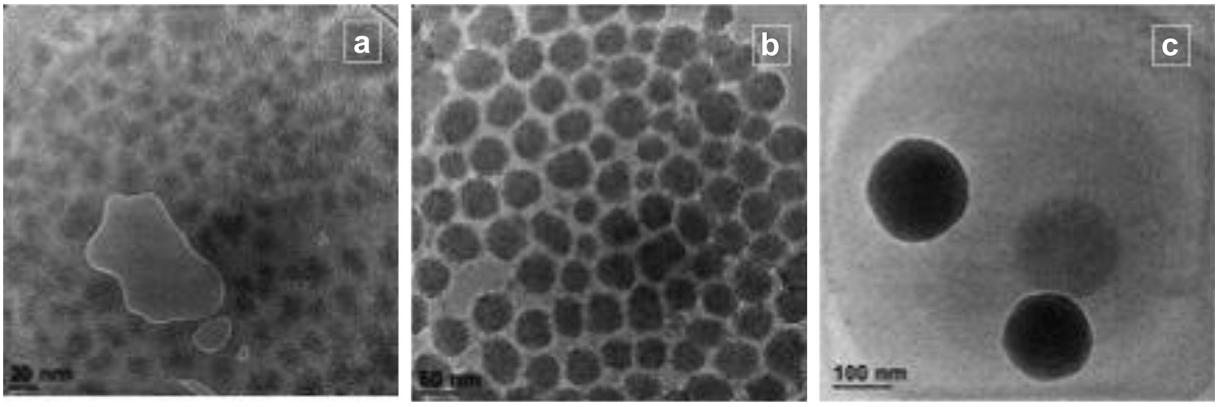

Fig. 1. TEM images of (a) S1, (b) S2 and (c) S3.

followed by the description of the silica used (S1, S2 or S3) and the silica content (1–40 wt. %).

Morphology of polyurethaneureas has been extensively investigated by AFM, TEM and SAXS studies. These studies indicated that depending on their compositions, hard segments in PTMO-based polyurethane-ureas are randomly oriented cylindrical domains 5–10 nm in width (and up to ca. 100 nm in length) and/or spherical domains in the order of 10–15 nm in diameter with interdomain spacing of 10–20 nm [36–38]. Hence, mean particle sizes of ca. 20–200 nm were particularly chosen to demonstrate the effect of particle sizes comparable to and bigger than the size of hard domains in the continuous polymeric matrix.

One of the key features that determines the enhancement in the performance and properties of the nanocomposites is the quality of the dispersion of the nano-sized particles in the polymeric matrix. Dispersion of the nanoparticles (intrinsically) depends on matrix–filler compatibility and surface energy of the particles as well as (extrinsically) the mixing method and conditions of the two phases. Silica particles could be specifically problematic due to presence of hydroxyl groups that lead to the formation of various sizes of agglomerates. Several studies indicate the aggregation and agglomeration of silica particles in polyurethane matrices regardless of filler size and silanol content [26,39–41]. Mean agglomerate size could reach up to 1 μm with respect to clustering of agglomerates at increased silica amounts. Common solutions to agglomeration have been surface modification of silica particles [30,42] and/or in-situ polymerization techniques [40], which could be efficiently employed up to certain loading levels. In this study, to avoid any drawback related to dispersion of silica nanoparticles in the polymeric matrix, silica sol was prepared and directly blended with the polymer solution in a common solvent. Solution blending was effective in avoiding the agglomeration of the silica nanoparticles and homogeneous blends were obtained prior to casting as demonstrated by the TEM image provided in Fig. 3. One drop of polymer/silica blend (TPU-20–S2-20) dried on a TEM grid clearly shows the random distribution of silica particles in the polymeric matrix.

Morphology of TPU/silica nanocomposite films was also studied by electron microscopy. SEM images of 20 wt. % silica (S1–S3) containing PTMO based TPU are reproduced in Fig. 4. Fig. 4(a) shows the smooth cross-section of neat TPU. SEM images of silica filled TPU samples given by Fig. 4(b–d) clearly show that no matter which particle size was employed, silica particles had a random but fairly homogeneous distribution throughout the polymeric matrix. The diffuse boundary between the polymer and the particles also indicated a strong interfacial interaction between two phases. TPU/silica nanocomposites with silica size lower than 100 nm resulted in even cross-section surfaces. However, widespread void formation in the polymer layer next to the filler surface was observed at cross-sections of the nanocomposites comprised of 200 nm silica particles (Fig. 4-d and -f). Similarly, extensive void formation was also revealed at cross-section SEM images of 40 wt. % silica loading (Fig. 4-e). It is interesting to note that silica particles retained their spherical shape and mean diameter after solution blending with the polyurethaneurea.

3.3. FTIR studies on nanocomposites

In order to understand the nature and extent of intermolecular interactions between silica and polyurethane–urea matrix, extensive FTIR investigations were performed on the nanocomposites. FTIR spectroscopy is a simple and useful tool in determining the

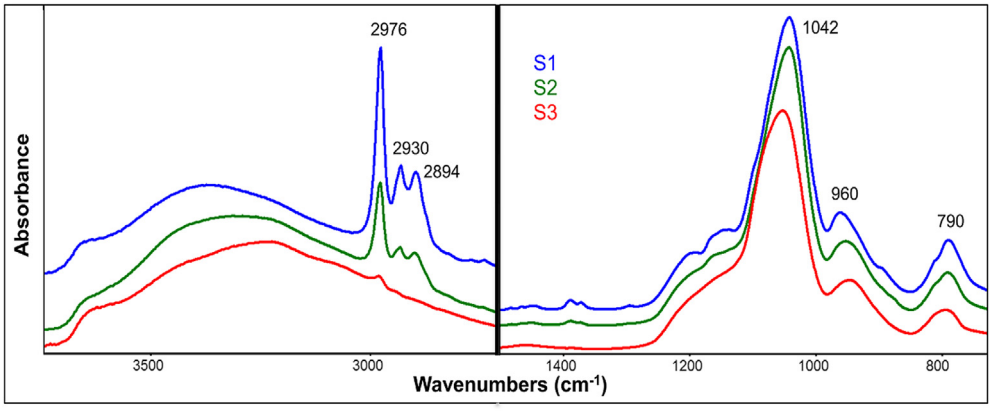

Fig. 2. FTIR–ATR spectra of dried colloidal silica designated as S1, S2 and S3.

Table 2
Compositions of TPU/colloidal silica composites.

Sample	Silica size (DLS/nm)	Silica content (wt.%)
TPU-20	–	–
TPU-20–S1-20	29	20
TPU-20–S2-20	74	20
TPU-20–S3-20	215	20
TPU-20–S2-1	74	1
TPU-20–S2-5	74	5
TPU-20–S2-10	74	10
TPU-20–S2-40	74	40

presence and the extent of possible interactions between silica and polyurethane–urea copolymer since changes in the hydrogen bonding character of polyurethane–urea matrix by the incorporation of silica nanoparticles can be easily detected by comparing the spectra of unfilled and silica filled samples. In this study our main focus was to identify the specific interactions between; (i) the hard segments and silica, and (ii) ether linkages present in the soft segment and silica. For this purpose, we examined specific regions in the IR spectroscopy, where strong absorptions were observed by urethane and urea groups (specifically N–H and C=O absorption bands), and ether (C–O–C) backbones. Peak shifts and shape changes especially at the hydroxyl and amine (3600–3000 cm^{-1}), carbonyl (1800–1500 cm^{-1}) and ether (1200–1000 cm^{-1}) regions, for the hard and soft segments respectively, are indications of an interaction between the silica and the matrix.

Fig. 5-a and -b, respectively, provide 3600–3000 cm^{-1} (N–H) and 1800–1600 cm^{-1} (C=O) regions of the FTIR spectra for base TPU-20 copolymer and TPU/silica nanocomposites containing 74 nm S2 silica as a function of filler amount. As can be seen in Fig. 5-a, TPU-20 (bottom spectrum) shows a symmetrical N–H absorption band in 3200–3400 cm^{-1} range. No dramatic change in the peak shape or position is observed for nanocomposites containing up to 20% by weight of silica. On the other hand, substantial broadening of the peak which covers the 3600–3000 cm^{-1} range is observed for 40% silica containing nanocomposite. This indicates a disruption in the interaction between N–H groups by the incorporation of large amounts of silica. Fig. 5-b shows the IR spectra of the carbonyl region. No major change was observed for the peak at 1633 cm^{-1}, which correspond to the ordered H-bonded urea carbonyls [43]. IR spectrum of neat polymer (TPU-20) shows a well-defined peak with maximum at 1718 cm^{-1} with a shoulder at 1701 cm^{-1}, which were attributed to the free and H-bonded urethane carbonyl bands. As seen in Fig. 5-b, the intensity of the shoulder at 1701 cm^{-1} increases at high silica loadings indicating an increase in hydrogen bonding association of urethane carbonyl groups in the presence of silica particles.

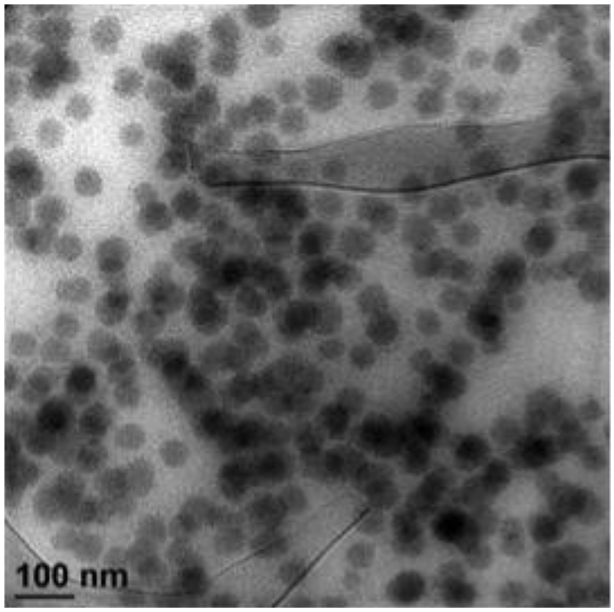

Fig. 3. TEM image of TPU-20–S2-20 blend dried on carbon coated Lacey formvar film supported in 300 mesh copper TEM grids.

FT-IR spectra in the ether region are presented in Fig. 6. Stretching vibrations of C–O–C group of neat PTMO-2K were observed at 1112 cm^{-1} (not displayed here). Therefore, the band observed at 1104 cm^{-1} in IR spectra of neat TPU-20 was attributed to the hydrogen bonding interaction between N–H and C–O–C groups. It should also be noted that similar band shift, which could be due to hydrogen bonding association of ether groups, was also observed in model studies of PTMO-2K/silica blends (not shown here). Unlike the N–H and C=O regions, when the ether region of the FTIR spectra is investigated, major changes in the peak positions and shapes are observed. As shown in Fig. 6, the peaks at ether region of the spectrum both broadened and shifted to lower wavenumbers as a function of the amount silica incorporation. Broadening of the peaks is attributed to the overlapping of Si–O–Si stretching of silica filler and C–O–C peaks of the polymeric matrix. The shift in the peak positions to the right, which also intensifies with increasing amount of silica filler in the matrix, is an indication of freshly formed hydrogen bonding between the hydroxyl groups on the silica surface and the oxygen atoms in the ether linkages of the PTMO backbone, due to increase in the surface contact area and number of hydroxyl groups. FTIR results indicate that silica nanoparticles interact mainly with the soft segment matrix; however, they do not significantly affect the hydrogen bonded hard domain structure. Consequently, silica seems to strongly interact with the soft segment of the polyether based TPU.

FTIR spectroscopy was also utilized to investigate the effect of silica particle size on the interaction with ether groups in TPU-20 at constant silica loading of 20% by weight. Change in the size of the silica filler did not indicate any remarkable change in the FTIR spectra in the N–H and C=O regions of the nanocomposites. On the other hand as shown in Fig. 7, ether peaks displayed broadening and shifted to shorter wavenumbers (from 1104 to 1080 cm^{-1}) as the silica particle size increased from 29 to 215 nm at constant loading of 20% by weight.

3.4. Thermal analyses by DSC and TGA

Thermal analyses of the nanocomposite films were performed by DSC and TGA measurements. Following the results of the FTIR studies, which indicated strong interaction between silica nanoparticles and the PTMO soft segment, model DSC studies were conducted on PTMO oligomer and its blend with 20% by weight of 74 nm silica (S2) in order to better understand this phenomena. DSC thermograms for these samples are reproduced in Fig. 8. PTMO oligomer displayed a well defined T_g at −80 °C and a sharp melting peak with maximum at 26 °C, which are in good agreement with the previously reported values [44]. Addition of 20% by weight S2 silica did not influence the position of the PTMO melting peak. However, heat of fusion decreased approximately by 20%, which may be expected.

Similar studies were also performed on TPU-20 and its nanocomposite with 20% by weight S2. As reproduced in Fig. 8, DSC thermogram of TPU-20 displayed a well defined T_g for the soft segment matrix at −78.5 °C but did not show any crystallization or melting peaks. TPU-20–S2-20 nanocomposite also showed a PTMO soft matrix T_g at −75.0 °C, but no melting transitions.

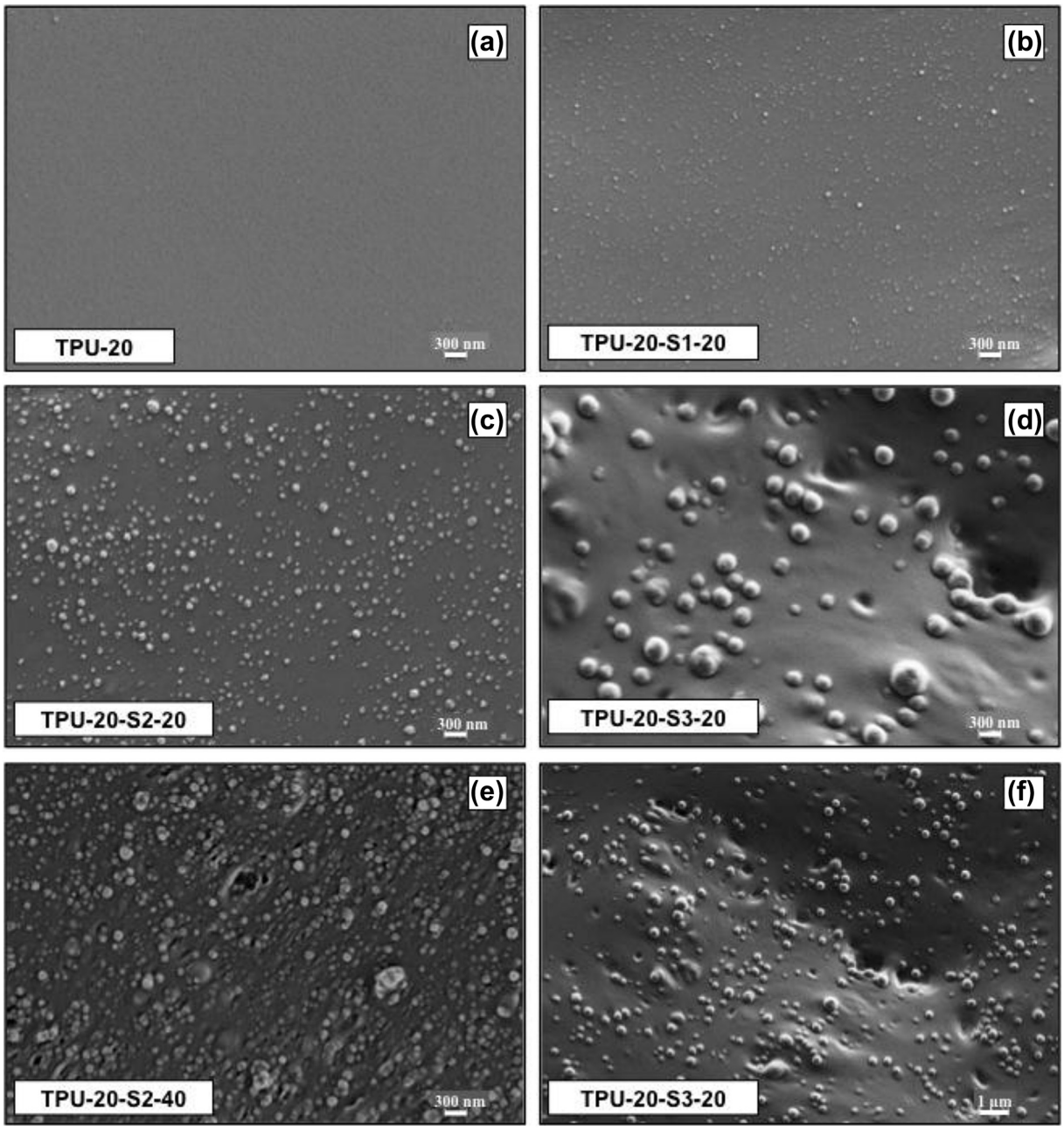

Fig. 4. SEM micrographs of TPU/silica nanocomposite cross-sections. 50 k× magnification: (a) TPU-20 neat polymer, (b) TPU-20–S1-20, (c) TPU-20–S2-20, (d) TPU-20–S3-20, (e) TPU-20–S2-40 and 20 k× magnification: (f) TPU-20–S3-20.

DSC analyses of a large number of nanocomposites were performed and the results are listed in Table 3. No significant change in the soft segment T_g was observed regardless of the silica size or the amount of incorporation. This phenomenon, which was also observed by several researchers [27,30,42,45], indicates no change in the soft segment mobility in the presence of silica particles dispersed in the polymeric matrix. Based on the interaction between the soft segments and silica nanoparticles that was evidenced by FTIR and homogeneous random distribution of the particles by SEM analyses, a decrease in the segmental mobility was expected. It is well known that in polyether urethanes and ureas, (N–H) groups form hydrogen bonds with both the carbonyl (C═O) of the hard segments and the oxygen (–O–) in the polyether soft segments [11]. We agree with the Sadeghi et al. [45] that sustained total segmental mobility in the presence of silica particles could be due to replacement of hydrogen bonding between N–H groups and ether groups with the hydrogen bonding between silica particles and ether groups in the soft segment of TPU. The disruption in the N–H absorption band and the significant band shifts in the ether region of the TPU in the presence of silica particles support this phenomenon. The increase in hydrogen bonding association of urethane carbonyl groups could be due to the presence of more N–H groups available for hydrogen bonding with this replacement. In addition, the T_g of the soft segments becomes broader and the heat capacity changes at glass transition (ΔC_p at T_g) show a steady decrease with increasing amount of silica. The decrease in heat capacity differences with increased filler content was expected since the filler does not contribute to the glass transition, and hence

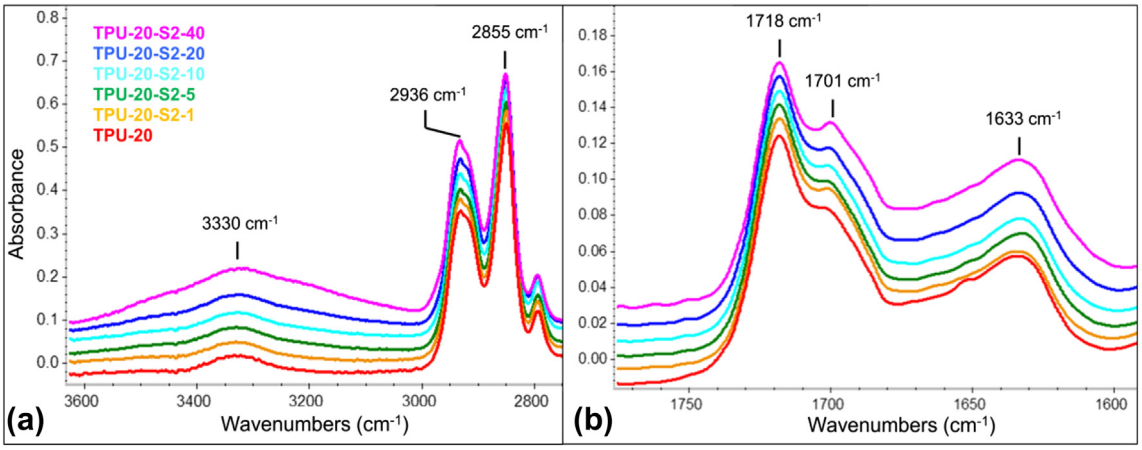

Fig. 5. FTIR investigation of (a) N–H and (b) carbonyl regions of neat TPU-20 and silica nanocomposites as a function of the amount of silica filler.

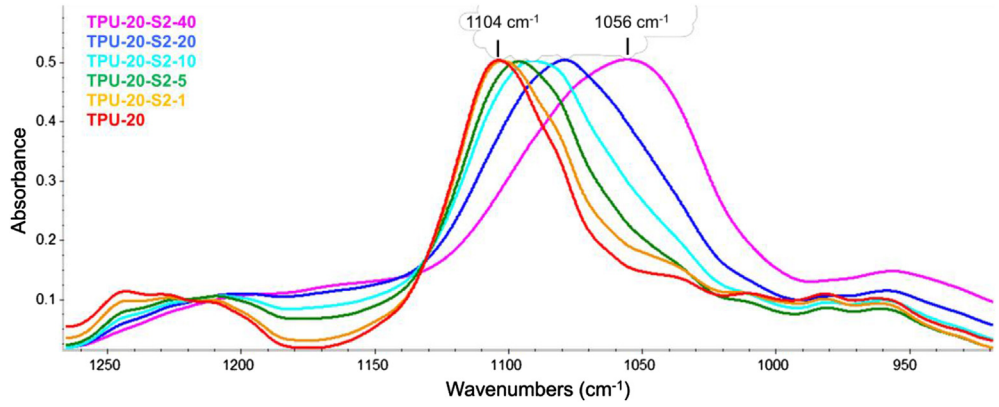

Fig. 6. Comparative FTIR spectra of the ether region for neat TPU-20 and its nanocomposites with S2.

the need of potential energy to create the volume for the segmental mobility decreases. However, the broadening of soft segment glass transition was attributed to the restricted mobility of soft segment chains [46].

TGA analyses were proposed to ascertain the thermal stability of polyether based TPU/silica nanocomposites. Fig. 9 displays thermogravimetric curves of prepared nanocomposites between 140 and 700 °C, which represents the region for more than 95% weight loss, under nitrogen atmosphere. The decomposition of polyether based neat TPU-20 starts at approximately 330 °C and single slope for weight loss is observed for the breakage of urethane/urea bonds, and subsequent thermal decomposition of the polyether polyol [47]. On the other hand, by silica addition a second slope appears up to 400 °C due to dehydroxylation of silanol groups and the degradation of the residual TEOS [48]. As clearly seen in Fig. 9, the slope of weight loss decreases by increasing the silica amount. The dashed lines indicating 50% weight loss clearly show that thermal resistance at high temperature is considerably enhanced in the presence of silica particles, and this was attributed to the thermal insulation effect of silica, as observed by Kim et al. [32,49]. Residual masses of the

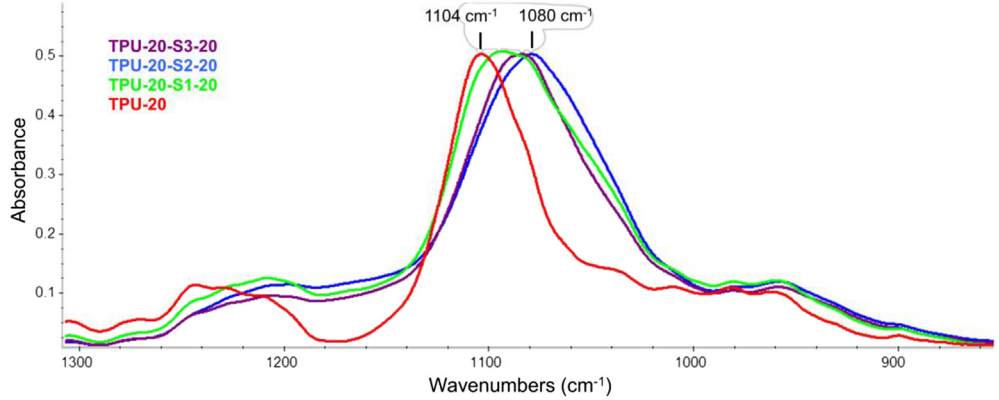

Fig. 7. Comparative FTIR spectra of the ether region for neat TPU-20 and its nanocomposites with 20% by weight S1, S2 and S3.

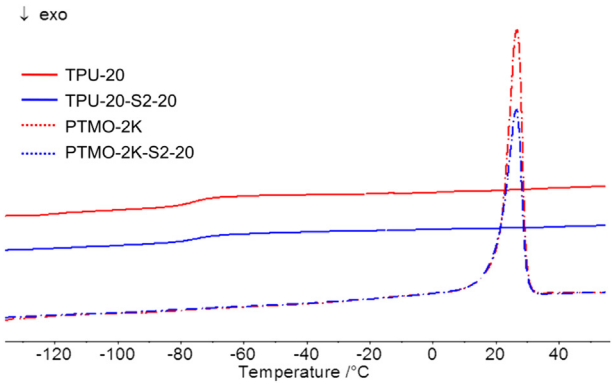

Fig. 8. DSC curves of PTMO, PTMO–S2-20, TPU-20 and TPU-20–S2-20.

nanocomposites after complete degradation at 650 °C are also listed in Table 3. These results compared well with the theoretical silica weight percentage of TPU/silica nanocomposites.

3.5. Stress–strain behavior

Segmented polyurethaneureas generally display excellent elastomeric properties with high tensile strengths and elongation at break values. To understand the effect of nanosilica incorporation on tensile properties, detailed stress–strain analysis of the nanocomposites were performed. Representative stress–strain curves for TPU-20 and its nanocomposites containing different amounts of 74 nm S2 silica are provided in Fig. 10. Detailed results regarding the analysis of the stress–strain studies are provided on Table 4.

As shown in Fig. 10 and Table 4, TPU-20 displays fairly nice elastomeric properties with a Young's modulus of 4.3 MPa, ultimate tensile strength of 27.8 MPa and elongation at break of 1000%. As expected, incorporation of silica resulted in an increase in the moduli of the nanocomposites as a function of the amount of the filler (except for TPU-20–S2-1) from 4.3 MPa for TPU-20 to 37.0 MPa for TPU-20–S2-40. In addition, an increasing trend in the tensile strength and a slight decrease in the elongation at break values of the nanocomposites as a function of silica content, up to

Table 3
Thermal properties of the TPUs/silica nanocomposites.

Sample	Filler		Residual mass (wt. %) at 650 °C	T_g (°C)	ΔC_p at T_g (J/g K)
	Size (nm)	ca. wt. %			
TPU-20	–	–	0.18	−75.8	0.387
TPU-20–S2-1	74	1	0.71	−75.0	0.384
TPU-20–S2-5	74	5	4.81	−74.3	0.377
TPU-20–S2-10	74	10	11.2	−76.1	0.369
TPU-20–S2-20	74	20	21.4	−75.1	0.293
TPU-20–S2-40	74	40	40.9	−74.6	0.144
TPU-20–S1-20	29	20	17.0	−74.2	0.274
TPU-20–S3-20	215	20	19.8	−75.4	0.335

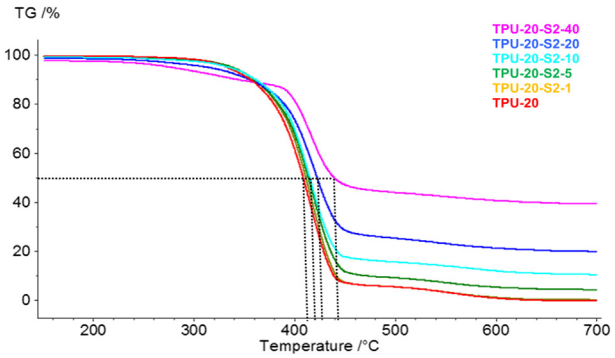

Fig. 9. TG curves of TPU/silica nanocomposites as a function of silica content. Dashed lines indicate the increase in thermal degradation temperature for 50% weight loss by silica addition.

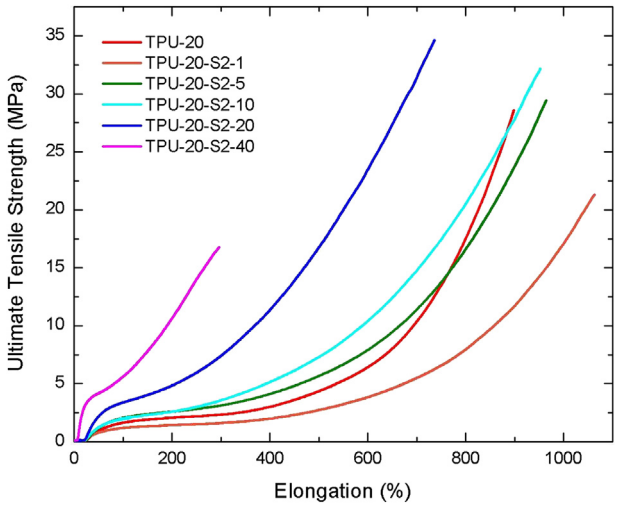

Fig. 10. Stress–strain curves of TPU-20 and its nanocomposites containing 1 to 40 wt. % of S2 colloidal silica.

Table 4
Tensile properties of TPU-20 and silica nanocomposites.

Sample	Filler		Tensile properties		
	wt.%	Size (nm)	*M* (MPa)	TS (MPa)	*E* (%)
TPU-20	–	–	4.3 ± 1.3	27.8 ± 3.7	1000 ± 30
TPU-20–S2-1	1	74	3.8 ± 1.0	27.7 ± 9.9	1070 ± 20
TPU-20–S2-5	5	74	6.7 ± 1.6	28.2 ± 2.4	970 ± 40
TPU-20–S2-10	10	74	6.7 ± 1.4	30.9 ± 2.9	950 ± 90
TPU-20–S2-20	20	74	10.8 ± 0.2	33.1 ± 3.9	800 ± 20
TPU-20–S2-40	40	74	37.0 ± 3.0	23.6 ± 5.4	430 ± 30
TPU-20–S1-20	20	29	10.7 ± 0.9	35.4 ± 2.9	850 ± 50
TPU-20–S3-20	20	215	8.6 ± 4.1	19.6 ± 3.1	830 ± 40

M: Young's modulus, TS: ultimate tensile strength at break, *E*: elongation at break.

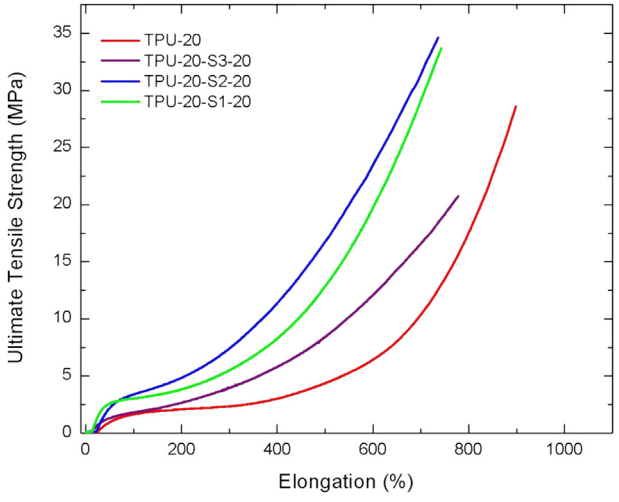

Fig. 11. Stress–strain curves of TPU-20 and nanocomposites containing 20 weight% S1, S2 and S3 colloidal silica.

Table 5
Nanomechanical properties of nanocomposites containing 20 wt. % silica.

Sample	h_c (nm)	E_r (MPa)	H (MPa)	Plasticity (ductility) index
TPU-20	920 ± 22	13.0 ± 0.6	1.6 ± 0.06	8.1
TPU-20-S1-20	960 ± 5	23.3 ± 0.4	2.5 ± 0.02	9.3
TPU-20-S2-20	971 ± 4	19.3 ± 0.3	2.0 ± 0.02	9.6
TPU-20-S3-20	963 ± 4	14.9 ± 0.2	1.6 ± 0.02	9.5

h_c – contact depth; E_r – reduced modulus; H – microhardness.

20% silica, were also observed. Interestingly, the sample containing only 1% by weight of nanosilica S2, TPU-20–S2-1 displayed a slightly lower modulus, approximately the same ultimate tensile strength and slightly higher elongation at break value when compared with TPU-20. Similar behavior was also observed by Bistričić et al. at 0.5 wt. % loading which was attributed to formation of bigger aggregates due to blending method [50]. Lee et al. also attributed the decrease in tensile strength above 5 wt. % silica loading to aggregate formation and decreased interfacial area yet TPU/silica nanocomposites were prepared in the presence of nanosilica [39]. However, we did not observe such a decreasing trend up to 20 wt. % silica loading. Very surprisingly, TPU-20–S2-40 displayed a reduction in ultimate tensile strength, which is still comparable with TPU-20, while retaining the elongation at break values above 400% at a modulus of 37 MPa. This reduction is most probably due to incomplete mixing of the filler and the matrix and formation of silica agglomerates and the voids formed between these agglomerates and the polymer layer as shown in SEM images provided in Fig. 4-e. These voids most probably lead to local stress concentrations and result in premature failure.

To understand the influence of silica particle size on tensile properties, stress–strain behavior of nanocomposites containing 20 wt. % S1, S2 and S3 silica was also investigated. Representative stress–strain curves for TPU-20 and the nanocomposites are provided on Fig. 11. Results are also summarized on Table 4. As expected, nanocomposites display higher Young's modulus values when compared with the TPU-20. More importantly they also show fairly good improvements in the ultimate tensile strengths, such as 35.4 MPa and 33.1 MPa for TPU-20–S1-20 and TPU-20–S2-20 respectively, when compared with 27.8 MPa for TPU-20. These results indicate that nanocomposites prepared from smaller particles with larger surface area per unit mass may be more attractive as reinforcing fillers in nanocomposites.

Nanomechanical tests were also performed by using quasi-static indents on TPU/silica nanocomposite films to understand the relationship between the hardness and fracture toughness with respect to filler size. Table 5 summarizes the mechanical responses in terms of average values of the reduced modulus (E_r) and hardness (H) for each sample, where both micro-hardness and contact stiffness (given by reduced modulus) increased as the silica particle size decreased in nanocomposites containing 20 wt. % silica loading.

The ratio of E_r/H is usually referred to as the plasticity or ductility index of the material, which reflects the relative amount of plastic indentation work [51] and correlates well with the fracture toughness [52]. As can be seen in Table 5, by 20 wt. % silica loading, plasticity and hence the fracture toughness of the TPU/silica nanocomposites could be enhanced regardless of the particle size.

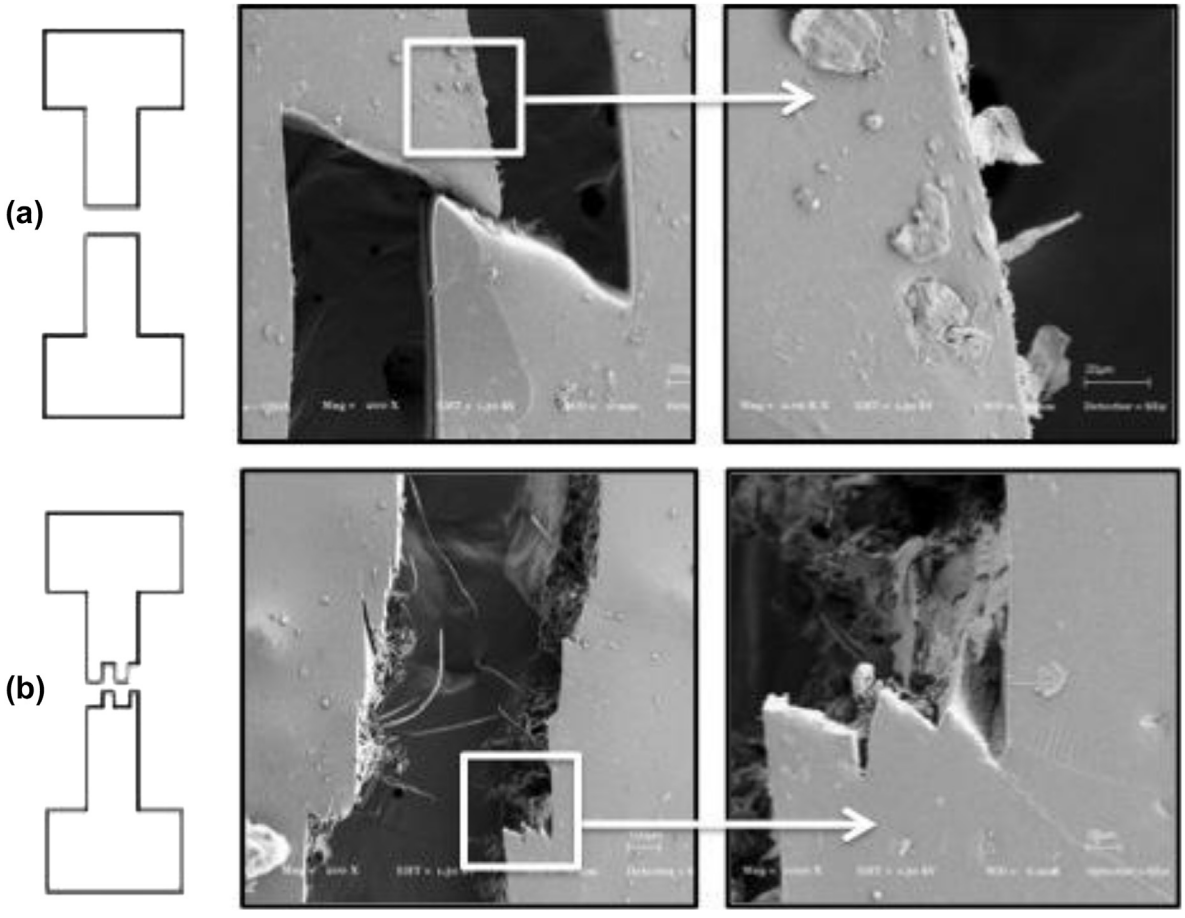

Fig. 12. SEM images of tensile-fractured surfaces of (a) TPU-20 and (b) TPU-20–S2-20.

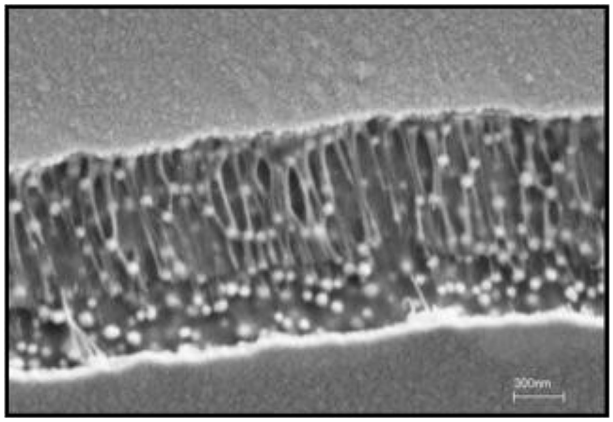

Fig. 13. SEM micrograph of a surface fracture on TPU-20–S2-20.

Another interesting observation was the difference in the structure or the topography of the ruptured surfaces after tensile tests, when unfilled and silica filled TPU-20 were compared. SEM micrographs of the ruptured surfaces for TPU-20 and TPU-20–S2-20 are shown in Fig. 12. Fig. 12-a shows a fairly clean surface for TPU-20 after rupturing. On the other hand Fig. 12-b shows a more complex and tethered rupture for TPU-20–S2-20, indicating a different fracture mode. Similar behavior was also observed in our previous studies on poly(silicone-urea)/silica composites, where increased rupture surface area leading to a reduction in stress concentration with silica loadings above 20 wt. % was reported [53]. In addition to these, strain induced fiber formation during rupture was clearly noticed with silica incorporation, indicating a clear interaction between polyurethane–urea copolymer and silica nanoparticles (Fig. 12-b).

Additional supporting observation on the formation of fibrous structures was also obtained when surface cracks induced on TPU-20–S2-20 was examined (Fig. 13). This SEM micrograph also reveals the contribution of the polymer–particle interaction on the distribution of the particles in the polymeric matrix and the homogeneous distribution of the silica nanoparticles obtained by solution blending that was employed for the preparation of TPU/silica nanocomposites.

4. Conclusions

Polyether based segmented polyurethane–urea/silica nanocomposites were effectively prepared by solution blending. Three different silica nanoparticles with average diameters of 29, 74 and 215 nm were prepared in our laboratories and used as fillers in amounts varying between 1 and 40 wt. %. Samples were characterized by FTIR spectroscopy, scanning electron microscopy (SEM), thermal analysis, tensile and nanoindentation to understand the influence of the nanoparticle size and content on the morphology as well as on the ultimate properties of the resultant nanocomposites.

Solution blending using a common solvent avoided the agglomeration of silica nanoparticles and produced homogeneous nanocomposites as evidenced by SEM results. Moreover, thermal resistance of polyether based TPU nanocomposites was improved in the presence of silica particles. FTIR studies showed stronger interaction between silica particles and the polyether matrix, as compared to the urethaneurea hard segments. However, soft segment T_g remained the same regardless of the silica size or the amount of incorporation. Even distribution of silica nanoparticles in the polyurethane–urea matrix enhanced the mechanical properties of the nanocomposites, which were primarily dependent on the size of the silica nanoparticles and amount of loading. Increased filler content up to about 20% by weight led to materials with higher elastic moduli and tensile strength values, while further increase resulted in loss of the elastomeric properties. Incorporation of silica nanoparticles with smaller particle sizes provided better enhancement in the modulus and tensile strength of the nanocomposites formed, while retaining their elastomeric properties. In addition to enhanced tensile properties, fracture toughness of the nanocomposites was improved, regardless of the silica particle size. We believe the reinforcement obtained was mainly due to the interactions between the silica nanoparticles and ether linkages of the polyether matrix of the copolymers.

Acknowledgments

Financial support from the Scientific and Technical Research Council of Turkey (TUBITAK) under contact number 109M073 is gratefully acknowledged.

References

[1] Schaefer DW, Justice RS. Macromolecules 2007;40(24):8501–17.
[2] Yao KJ, Song M, Hourston DJ, Luo DZ. Polymer 2002;43(3):1017–20.
[3] Zou H, Wu S, Shen J. Chemical Reviews 2008;108(9):3893–957.
[4] Koerner H, Liu W, Alexander M, Mirau P, Dowty H, Vaia RA. Polymer 2005;46(12):4405–20.
[5] Paul DR, Robeson LM. Polymer 2008;49(15):3187–204.
[6] Pham JQ, Mitchell CA, Bahr JL, Tour JM, Krishanamoorti R, Green PF. Journal of Polymer Science Part B: Polymer Physics 2003;41(24):3339–45.
[7] Luong ND, Hippi U, Korhonen JT, Soininen AJ, Ruokolainen J, Johansson L-S, et al. Polymer 2011;52(23):5237–42.
[8] Dan CH, Lee MH, Kim YD, Min BH, Kim JH. Polymer 2006;47(19):6718–30.
[9] Zha W, Han CD, Moon HC, Han SH, Lee DH, Kim JK. Polymer 2010;51(4):936–52.
[10] Saeed K, Park S-Y, Lee H-J, Baek J-B, Huh W-S. Polymer 2006;47(23):8019–25.
[11] Yilgor E, Burgaz E, Yurtsever E, Yilgor I. Polymer 2000;41(3):849–57.
[12] Das S, Cox DF, Wilkes GL, Klinedinst DB, Yilgor I, Yilgor E, et al. Journal of Macromolecular Science Part B-Physics 2007;46(5):853–75.
[13] Oertel G. Polyurethane handbook. 2nd ed. New York: Hanser; 1993.
[14] Szycher M. Handbook of polyurethanes. Washington D.C.: CRC Press; 1999.
[15] Lee S. Thermoplastic polyurethane markets in the EU: production, technology, applications and trends. UK: Rapra Technology Limited; 1998.
[16] Chen TK, Tien YI, Wei KH. Polymer 2000;41(4):1345–53.
[17] Choi WJ, Kim SH, Jin Kim Y, Kim SC. Polymer 2004;45(17):6045–57.
[18] Potschke P, Haussler L, Pegel S, Steinberger R, Scholz G. Kgk-Kautschuk Gummi Kunststoffe 2007;60(9):432–7.
[19] Russo P, Acierno D, Spena P. Rheological behaviour, mechanical properties and morphological aspects of thermoplastic polyurethane reinforced with multiwalled carbon nanotubes. In: Damore A, Acierno D, Grassia L, editors. 5th International conference on times of polymers top and composites. vol. 1255. Melville: Amer Inst Physics; p. 168–71.
[20] Hunley MT, Potschke P, Long TE. Macromolecular Rapid Communications 2009;30(24):2102–6.
[21] Barick AK, Tripathy DK. Journal of Applied Polymer Science;124(1):765–80.
[22] Powers DS, Vaia RA, Koerner H, Serres J, Mirau PA. Macromolecules 2008;41(12):4290–5.
[23] Jauregui-Beloqui B, Fernandez-Garcia JC, Orgiles-Barcelo AC, Mahiques-Bujanda MM, Martin-Martinez JM. Journal of Adhesion Science and Technology 1999;13(6):695–711.
[24] Vega-Baudrit J, Sibaja-Ballestero M, Vázquez P, Torregrosa-Maciá R, Miguel Martín-Martínez J. International Journal of Adhesion and Adhesives 2007;27(6):469–79.
[25] Torró-Palau AM, Fernández-García JC, César Orgilés-Barceló A, Martín-Martínez JM. International Journal of Adhesion and Adhesives 2001;21(1):1–9.
[26] Vega-Baudrit J, Navarro-Bañón V, Vázquez P, Martín-Martínez JM. International Journal of Adhesion and Adhesives 2006;26(5):378–87.
[27] Petrovic ZS, Javni I, Waddon A, Banhegyi G. Journal of Applied Polymer Science 2000;76(2):133–51.
[28] Petrovic ZS, Javni I, Waddon A, Soc Plast E. Polyurethane elastomers with nano-fillers; 1998.
[29] Javni I, Zhang W, Karajkov V, Petrovic ZS, Divjakovic V. Journal of Cellular Plastics 2002;38(3):229–39.
[30] Chen G, Zhou S, Gu G, Yang H, Wu L. Journal of Colloid and Interface Science 2005;281(2):339–50.
[31] Gerard JF, Kaddami H, Pascault JP. Manchester; 1997.
[32] Jeon HT, Jang MK, Kim BK, Kim KH. Colloids and Surfaces A: Physicochemical and Engineering Aspects 2007;302(1–3):559–67.
[33] Bae CY, Park JH, Kim EY, Kang YS, Kim BK. Journal of Materials Chemistry 2011;21(30):11288–95.

[34] Stöber W, Fink A, Bohn E. Journal of Colloid and Interface Science 1968;26(1):62–9.
[35] Costa CAR, Leite CAP, Galembeck F. The Journal of Physical Chemistry B 2003;107(20):4747–55.
[36] Garrett JT, Siedlecki CA, Runt J. Macromolecules 2001;34(20):7066–70.
[37] McLean RS, Sauer BB. Macromolecules 1997;30(26):8314–7.
[38] Desper CR, Schneider NS, Jasinski JP, Lin JS. Macromolecules 1985;18(12):2755–61.
[39] Lee S-I, Hahn YB, Nahm KS, Lee Y-S. Polymers for Advanced Technologies 2005;16(4):328–31.
[40] Chen Y, Zhou S, Yang H, Gu G, Wu L. Journal of Colloid and Interface Science 2004;279(2):370–8.
[41] Zhou S, Wu L, Sun J, Shen W. Progress in Organic Coatings 2002;45(1):33–42.
[42] Chen G, Zhou S, Gu G, Wu L. Colloids and Surfaces A: Physicochemical and Engineering Aspects 2007;296(1–3):29–36.
[43] Yilgor E, Yilgor I, Yurtsever E. Polymer 2002;43(24):6551–9.
[44] Hu CB, Ward RS, Schneider NS. Journal of Applied Polymer Science 1982;27(6):2167–77.
[45] Sadeghi M, Semsarzadeh MA, Barikani M, Ghalei B. Journal of Membrane Science 2011;385(1–2):76–85.
[46] Xu YJ, Petrovic Z, Das S, Wilkes GL. Polymer 2008;49(19):4248–58.
[47] Huang SL, Lai JY. Journal of Applied Polymer Science 1995;58(10):1913–23.
[48] Jafarzadeh M, Rahman IA, Sipaut CS. Journal of Sol-Gel Science and Technology 2009;50(3):328–36.
[49] Kim BK, Seo JW, Jeong HM. Macromolecular Research 2003;11(3):198–201.
[50] Bistričić L, Baranović G, Leskovac M, Bajsić EG. European Polymer Journal;46(10):1975–87.
[51] Greenwood JA, Williamson JBP. Proceedings of the Royal Society of London. Series A. Mathematical and Physical Sciences 1966;295(1442):300–19.
[52] Tanaka K. Journal of Materials Science 1987;22(4):1501–8.
[53] Yilgor E, Eynur T, Kosak C, Bilgin S, Yilgor I, Malay O, et al. Polymer 2011;52(19):4189–98.